

# 1 Earthquake clustering controlled by shear zone interaction

2  
3 Mildon, Zoë K.<sup>1,\*</sup>, Roberts, Gerald P.<sup>2</sup>, Faure Walker, Joanna P.<sup>3</sup>, Beck, Joakim<sup>4</sup>,  
4 Papanikolaou, Ioannis<sup>5</sup>, Michetti, Alessandro M.<sup>6</sup>, Toda, Shinji<sup>7</sup>, Iezzi, Francesco<sup>2</sup>,  
5 Campbell, Lucy<sup>1</sup>, McCaffrey, Kenneth J.W.<sup>8</sup>, Shanks, Richard<sup>9</sup>, Vittori, Eutizio<sup>10</sup>,  
6

7 1. University of Plymouth, UK

8 2. Birkbeck, University of London, UK

9 3. University College London, UK.

10 4. King Abdullah University of Science and Technology (KAUST), Saudi Arabia.

11 5. Agricultural University of Athens, Greece.

12 6. Università degli Studi dell'Insubria, Como, Italy.

13 7. Tohoku University, Sendai, Japan.

14 8. University of Durham, UK.

15 9. Scottish Universities Environmental Research Centre, East Kilbride, UK

16 10. Istituto Superiore per la Prevenzione e la Ricerca Ambientale, Rome, Italy.

17  
18 \* Corresponding author: Zoë Mildon, zoe.mildon@plymouth.ac.uk  
19

## 20 Abstract

21 Earthquakes are known to cluster in time, from historical and palaeoseismic  
22 studies, but the mechanism(s) responsible for clustering, such as evolving  
23 dynamic topography, fault interaction, and strain-storage in the crust are  
24 poorly quantified, and hence not well understood. We note that differential  
25 stress values are (1) output by calculations of fault interaction, and (2) needed  
26 as input to calculate strain-rates for viscous shear zones that drive slip on  
27 overlying active faults. However, these two separate fields of geoscience have  
28 never been linked to study earthquake clustering. Here we quantify the links  
29 between these fields, and replicate observations of earthquake clustering from  
30 a <sup>36</sup>Cl cosmogenic study of six interacting active normal faults. We derive  
31 differential stress change values from Coulomb stress transfer calculations,  
32 and use these values in a viscous flow law for dislocation creep to calculate  
33 changes in strain-rate for shear zones, and slip-rates and earthquake  
34 recurrence on overlying active faults. Our quantification of clustering, verified  
35 with observations, reveals how brittle and viscous processes in the upper and  
36 lower crust interact, driving temporal changes in slip-rate and seismic hazard.

37 It has long been known that earthquake recurrence is not strictly periodic, with  
38 evidence for temporal earthquake clusters lasting hundreds to thousands of years  
39 and containing several large-magnitude ( $M_w > 6$ ) earthquakes<sup>1</sup>. Currently, we lack  
40 understanding of what controls such aperiodicity. This confounds our attempts to  
41 mitigate seismic hazard, because the greater the aperiodicity, the greater the  
42 uncertainty in recurrence intervals, a vital input for time-dependent probabilistic  
43 seismic hazard assessment<sup>2</sup>. Boundary conditions driving the deformation are likely  
44 to be constant over the timescales of clustering of a few millennia or less<sup>3,4</sup>, therefore  
45 it must be that the faulting process itself induces clustered activity and we investigate  
46 this herein.

47

48 An important insight comes from recent work<sup>3</sup>, consistent with an old, but classic  
49 idea<sup>5</sup>, that slip on brittle faults in the upper crust is driven by the slip on underlying  
50 viscous shear zones in the lower crust. The recent work revealed a correlation  
51 between strain-rates derived from measurements of slip-rates on surface fault  
52 scarps<sup>6</sup> and topographic elevation in the Italian Apennines extensional region, (Fig.  
53 1). The strain-rates were averaged over a time period ( $15 \pm 3$  ka) longer than the  
54 timescale of clustered slip. The correlation takes the form of a power law, where  
55 strain-rate,  $\dot{\epsilon}$  is related to the elevation,  $h$ , in the form  $\dot{\epsilon} \propto h^n$ , with  $n = 3.26$ . These  
56 authors<sup>3</sup>, considered that  $h$  contributes to the differential stresses driving the  
57 deformation, alongside tectonic forcing, because  $h$  contributes to the vertical stress.  
58 Hence  $\dot{\epsilon} \propto h^n$  resembles the classic quartz flow law for dislocation creep in quartz  
59 shown in equation (1)<sup>7</sup>, where,  $\dot{\epsilon}$  is strain rate,  $A$  is a material parameter,  $fH_2O$  is  
60 water fugacity,  $m$  is the water fugacity exponent,  $\sigma$  is the differential stress,  $n$  is the  
61 stress exponent,  $Q$  is the activation energy,  $R$  is the ideal gas constant, and  $T$  is  
62 absolute temperature.

63

$$64 \quad \dot{\epsilon} = AfH_2O^m \sigma^n \exp(-Q/RT) \quad (1)$$

65

66 The power law form  $\dot{\epsilon} \propto \sigma^n$  implies that strain-rates accommodated by the brittle  
67 faults are driven by the strain-rate of the viscous deformation on underlying shear  
68 zones.

69

70 The question that arises is what would result if the differential stresses within  
71 underlying shear zones changed due to shear zone interaction? Slip on a shear zone

72 or brittle fault will induce elastic strain in the surrounding rocks, including minerals  
73 within neighbouring mylonitic shear zones, changing the stress (Fig. 2). Values for  
74 differential stress can be calculated<sup>8,9</sup> via Coulomb stress calculations. These values  
75 can then be used to calculate implied changes in shear zone strain-rates using a  
76 quartz flow law<sup>7</sup>. These changes in strain-rate will affect the slip rates of the overlying  
77 faults; we investigate if this produces slip-rate changes of the timescale and  
78 magnitude associated with earthquake clustering.

79

80 We have no direct measurements of strain-rate changes over a few centuries or  
81 millennia for shear zones in the lower crust. However, it has been argued above that  
82 strain-rates from brittle faults reveal strain-rates in underlying shear zones<sup>3</sup> (Fig. 1).  
83 We measure slip-rate changes on brittle faults using *in situ* <sup>36</sup>Cl cosmogenic  
84 exposure analyses on bedrock fault scarps. This reveals that periods of rapid slip on  
85 some faults (clusters) are contemporaneous with periods of slow slip (anticlusters) on  
86 others. We input the timing and magnitude of rapid slip into stress transfer models,  
87 using the output stress changes as inputs for viscous flow calculations for dislocation  
88 creep to constrain strain-rates changes for shear zones beneath faults experiencing  
89 slow slip. Our aim is to examine whether the magnitude of strain-rate decrease is of  
90 the correct magnitude to explain the slow slip.

91

## 92 Cosmogenic analyses of fault scarps reveal millennial earthquake clusters

93 The measurements in our study come from the Italian Apennines, a region of  
94 extension since 2-3 Ma<sup>6,10</sup>, with active normal faults deforming a pre-existing alpine  
95 fold and thrust belt<sup>11,12</sup>. Geodetic and seismological observations confirm extension  
96 rates of ~3 mm/yr across the Apennines<sup>13,14</sup>. Historical and instrumental seismicity  
97 indicates that large ( $M_w$ 5.5-7.0) magnitude normal faulting earthquakes occur<sup>15,16</sup> and  
98 produce surface carbonate fault scarps<sup>6,17-19</sup> (Fig. 1e). The surface fault scarps have  
99 been preserved since the demise of the last glacial maximum (LGM, 15 ±3 ka), due  
100 to a reduction in erosion rates relative to throw rates<sup>20</sup> (Fig. 1). These scarps have  
101 been studied with *in situ* <sup>36</sup>Cl cosmogenic exposure analyses, confirming the post-  
102 LGM slope stabilisation age and fault slip rate histories that are variable during the  
103 Holocene<sup>21,22</sup>. In places, dense <sup>36</sup>Cl sampling has revealed correlation of high slip-  
104 rate events with the timing of damaging earthquakes that affected Rome<sup>23</sup>.

105

106 We focus on a single normal fault in the central Apennines because this fault recently  
107 ruptured after an anomalously long elapsed time since the last earthquake. The Mt.  
108 Vettore fault ruptured to the surface in the August-October 2016 sequence, which

109 included Mw 6.2, 6.1 and 6.6 earthquakes (Fig. 1e). Paleoseismological studies  
110 suggest that before 2016, this SW-dipping active normal fault had not ruptured to the  
111 surface for several thousand years, with suggestions of the elapsed time ranging  
112 between 1316-4155 years BP<sup>24</sup>, and 6446 +1330/-2660 years BP<sup>25</sup>. Interestingly,  
113 during this period, five other nearby faults have ruptured to the surface in damaging  
114 historical earthquakes with elapsed times of less than a few hundred years, (1349  
115 AD, Fiamignano fault; 1639 AD, Laga fault; 1703 AD, Norcia and Barete faults; 1997  
116 AD Mt Le Scalette fault; late Holocene, Leonessa fault), revealed by historical  
117 accounts, paleoseismic studies and <sup>36</sup>Cl studies<sup>23,26-32</sup>. A pattern emerges where one  
118 fault has not slipped, whilst its neighbours have slipped in the same time period. It is  
119 this intriguing observation that motivated our study.

120

121 We sampled the six faults for <sup>36</sup>Cl cosmogenic analyses prior to the 2016  
122 earthquakes, sampling up the fault plane and within shallow (<~1m) trenches parallel  
123 to the slip-vector. We constrained the sample sites with geological mapping and  
124 topographic surveys. These data confirm the exposed fault scarps are formed solely  
125 due to tectonic slip and not erosional/depositional processes. We statistically inferred  
126 the slip implied by the <sup>36</sup>Cl data using a Bayesian Markov chain Monte Carlo (MCMC)  
127 approach<sup>23</sup>. The results show evidence of slip-rate changes that imply temporal  
128 earthquake clustering (Fig. 3). We note that rapid slip occurred synchronously on the  
129 SW and NE flank of the Apennines (e.g. compare slip in the last few thousand years  
130 on the Laga and Fiamignano faults). This rules out the hypothesis that activity  
131 migrates, producing clustering, due to least-work constraints imposed by spatial  
132 changes in dynamic topography<sup>22</sup>.

133

134 We have four key observations from our statistical modelling of the <sup>36</sup>Cl data that help  
135 to reveal the cause of the slip-rate changes (Fig. 3): (1) the slip-rate on the Mt.  
136 Vettore fault slows at ~4 ka; (2) the other faults accelerated, starting at ~3.5 ka; (3)  
137 prior to ~4 ka, the Mt. Vettore fault underwent a high slip-rate phase relative to its  
138 slip-rate averaged since ~17.5 ka; (4) prior to ~3.5 ka, the other faults had slip-rates  
139 that were relatively low compared their 15 ±3 kyrs average slip rate. Our  
140 observations are consistent with existing paleoseismic observations<sup>25,28</sup>. The  
141 question that arises is whether the underlying viscous shear zones were also  
142 involved in the interaction, slowing or accelerating in tandem with their overlying  
143 brittle faults.

144

145 Calculating the effect of fault interaction on stress transfer and strain rate changes

146 To quantify interactions between the faults and the viscous shear zones, we  
147 extracted the amount of slip on each fault in the time period from ~3.5 ka to 2015 AD,  
148 and prior to ~3.5 ka. We modelled the Coulomb stress transfer (CST)<sup>9</sup> implied by the  
149 amount of slip derived from the <sup>36</sup>Cl modelling in each time period (e.g. Fig. 3). We  
150 calculate CST on neighbouring faults and shear zones (so-called receiver  
151 faults/shear zones) (Fig. 4), and convert to differential stress<sup>8</sup> for shear zones. We  
152 concentrate our analysis on the Mt. Vettore and Leonessa faults, because these  
153 faults are located centrally in the study area and receive stress from slip on both  
154 along-strike and across-strike faults that we can constrain with <sup>36</sup>Cl and paleoseismic  
155 data<sup>28,33</sup> (Fig. 3). The calculations reveal stress-loading histories during temporal  
156 earthquake anticlusters, on the Mt. Vettore and Leonessa faults and underlying shear  
157 zones (Fig. 4). We discuss the results for faults and shear zones separately.

158

159 For faults, we do not find a consistent pattern of increasing or decreasing CST during  
160 anticlusters. For the Mt. Vettore fault, we find that the CST from neighbouring fault  
161 slip became mostly positive during its quiescence from ~3.5 ka to present (Fig. 4aii),  
162 before it ruptured in 2016<sup>34</sup>. An earthquake after a relatively-long elapsed time is  
163 perhaps intuitively expected because faults will be loaded through time by far-field  
164 tectonic forces<sup>35</sup>, and CST may positively load the fault<sup>36</sup>. However this intuitive view  
165 breaks down for the Leonessa fault, because the CST became increasingly negative  
166 during its low slip-rate time period from 17 ka to ~3.5 ka (Fig. 4iv). Despite the  
167 negative CST, the Leonessa fault did not cease activity, with <sup>36</sup>Cl data indicating an  
168 accumulation of 6.5 m slip between 3.5 to present, with historical constraints  
169 narrowing this to 3.5 to 0.7 ka, proving it is a Holocene active fault<sup>31</sup>. Overall, it  
170 appears that CST on brittle faults does not directly explain why brittle faults  
171 experience anticlusters and then rupture, as the loading can be positive or negative  
172 due to fault interaction.

173

174 For shear zones we find a consistent pattern of stress loading during anticlusters.  
175 During the two anticlusters we study, the magnitudes of differential stress change for  
176 shear zones are in the range of -2.8 to -4.0 MPa. This is significant given that we  
177 expect the differential stress in shear zones to be only ~10 MPa, and essentially  
178 constant over the ~15-24 km depth range, from investigations of exhumed  
179 extensional shear zones<sup>37</sup> (Figs. 4ai and 4iii). The Mt. Vettore shear zone  
180 experienced a stress reduction of up to -2.8 MPa between 3.5 ka and 2015 AD. The  
181 Leonessa shear zone experienced a stress reduction of up to -4.0 MPa between 17  
182 and 3.5 ka. This observation that differential stress change was negative when both

183 overlying faults had very low slip-rates (antoclusters) prompted us to investigate  
184 whether the magnitudes of differential stress reduction generate strain-rate changes  
185 comparable to our observations from  $^{36}\text{Cl}$ .

186

187 To calculate the implied change in strain-rate for each shear zone within the two  
188 antoclusters, we input the reductions of differential stress into Equation 1, using  
189 appropriate values for other variables<sup>7</sup>. Assuming the patch with the largest stress  
190 decrease is the rate-limiting element, it is implied that strain-rates would have  
191 decreased from  $1.5 \times 10^{-16}$  to  $5.0 \times 10^{-17}$  on the Mt. Vettore shear zone between 3.5  
192 ka and 2015 AD, whilst for the Leonessa shear zone strain-rate would have been  
193 decreased from  $1.5 \times 10^{-16}$  to  $2.8 \times 10^{-17}$  between 17-3.5 ka (Figs. 4a,b). Thus, both  
194 shear zones were still active during periods of earthquake quiescence, albeit with  
195 reduced strain-rates. Therefore earthquake ruptures on the overlying faults at the  
196 end of both antoclusters suggests that the impact of stress changes on the brittle  
197 faults, either positive or negative, is overwhelmed through time by slip and loading  
198 associated with the underlying viscous shear zones.

199

200 To compare the effect of the implied strain-rate changes with our  $^{36}\text{Cl}$  measurements  
201 of the natural system, we converted the strain-rates in the shear zones into implied  
202 slip-rates on the overlying brittle faults, and compared them with the observed slip-  
203 rates (Figs. 3 and 4). We used the slip measured over the total time period  
204 constrained with  $^{36}\text{Cl}$  as a measure of the stable long-term slip-rate<sup>3</sup>. We compare  
205 these long-term slip-rates with slip-rates during clusters/antoclusters constrained by  
206 the  $^{36}\text{Cl}$  data. This allows us to calculate slip-rate enhancement factors (SRE) that  
207 describe how much the slip-rates over millennia were enhanced (SRE >1) or  
208 impeded (SRE <1) compared to the long-term slip-rates (Fig. 4c). SRE values range  
209 between <1 to >4 in both the measured and implied slip-rate datasets. We find that  
210 the implied slip-rate histories resemble those derived from  $^{36}\text{Cl}$  (Fig. 4ci), as does  
211 implied SRE compared to measured SRE (Fig. 4cii;  $R^2 = 0.985$ ). This implies that our  
212 novel approach outlined herein is able to explain key slip-rate observations from the  
213 natural system, providing insight into the processes that drive earthquake clustering  
214 and anticlustering.

215

### 216 Implications for seismic hazard and continental extension

217 Earthquake clustering confounds our ability to mitigate seismic hazard because the  
218 greater the aperiodicity in recurrence intervals in fault-based time-dependent hazard  
219 assessments, the greater the uncertainty that will need to be communicated

220 probabilistically with regard to recurrence of expected ground accelerations within  
221 stated time periods<sup>2</sup>. Greater uncertainty may lead to reluctance with regard to  
222 implementing costly mitigation strategies. One approach to explain the aperiodicity is  
223 to suggest that the processes that control slip are multiple, complex, interacting, and  
224 difficult to quantify, and the system may be considered as approaching random  
225 behavior<sup>38</sup>. However, the key implication herein is that, instead, earthquake  
226 clustering appears to have a dominant, quantifiable cause, and is therefore not  
227 random. Our results suggest that viscous shear zones slow or accelerate due  
228 to changes in differential stress produced by slip on nearby viscous shear zones and  
229 brittle faults. Our results appear to rule out the notions that upper crustal brittle fault  
230 interaction<sup>39</sup>, or least-work constraints imposed by dynamic topography<sup>21</sup> are the sole  
231 controls responsible for earthquake clustering. Our interpretation, where shear zone  
232 strain-rates change due to stress transfer altering the differential stress, may be  
233 linked to suggestions that tectonic strain is stored during anticlusters<sup>40,41</sup>, and/or may  
234 be linked to the mechanism by which microstructural evolution leads to shear-zone  
235 strengthening during anticlusters if this process occurs<sup>42</sup>. Clearly, more work is  
236 needed, but the links we have made between geomorphic offsets, cosmogenic dating  
237 of faults scarps, calculations of stress transfer, and viscous flow laws, provide  
238 important new insights into seismic hazard that go beyond what can be achieved by  
239 simply studying instrumental seismicity. In particular, our results suggest that we  
240 should expect slip-rate changes through time on the timescale of earthquake  
241 clustering, as these are the natural consequence of fault and shear zone interactions.  
242 These slip-rate changes will alter earthquake recurrence rates and should be  
243 included in seismic hazard calculations. This approach warrants further study and we  
244 suggest that an independent test of our model will require calculations of stress  
245 change due to slip within time periods with precise time constraints such as we  
246 provide herein. Such studies will improve our ability to use values of slip-rate  
247 variability and aperiodic earthquake recurrence within fault-based probabilistic  
248 seismic hazard assessments<sup>42</sup>.

249

## 250 **Acknowledgements**

251 This work was funded by NERC Standard Grant NE/I024127/1, NERC Large Grant  
252 NE/J016497/1, NERC Standard Grant NE/E01545X/1, NERC Studentship  
253 NE/L501700/1, NERC Urgency Grant NE/P01660X/1 (EEFIT Reconnaissance  
254 Mission to the Amatrice, Italy, 24/09/2016 Earthquake), Japan Society for the  
255 Promotion of Science (JSPS) Short Term Fellowship PE15776, the Jeremy Willson  
256 Charitable Trust, Geological Society Mike Coward fieldwork fund, and GBSF (Great

257 Britain Saskawa Foundation) grant 4602. We thank Laura Gregory for discussions,  
258 participation in fieldwork, chemical analyses and preparation of the  $^{36}\text{Cl}$  samples. We  
259 thank Patience Cowie for many discussions and ideas that helped to lead us to this  
260 study. We thank Andrew Watson and Luke Wedmore for their assistance in the field  
261 during sampling. We thank Richard Phillips for setting up the cosmogenic lab at the  
262 University of Leeds where the sample preparation took place. The cosmogenic data  
263 is published online in a repository and is freely available for download at  
264 <https://www.bgs.ac.uk/services/ngdc/accessions/index.html#item128345>.

265

## 266 **Contributions**

267 ZM performed all the Coulomb stress modelling, helped to locate, sample and  
268 process some of the  $^{36}\text{Cl}$  data, helped to develop our approach to fault/shear-zone  
269 interactions and use of the quartz flow law, and co-wrote the manuscript, providing  
270 diagrams and supplements. GR provided background knowledge of the regional  
271 geology, seismicity and geodesy, helped to locate and sample  $^{36}\text{Cl}$  sites, overseeing  
272 field constraints on all sites, modelled the  $^{36}\text{Cl}$  data, helped to develop our approach  
273 to fault/shear-zone interactions and use of the quartz flow law, and our comments on  
274 seismic hazard, and co-wrote the manuscript, providing diagrams and supplements.  
275 JFW calculated strain rates for the region, helped with fieldwork, and helped to  
276 develop our approach to fault/shear-zone interactions, quartz flow modelling and our  
277 comments on seismic hazard. JB led development of our approach to modelling slip  
278 histories from the  $^{36}\text{Cl}$  data, and helped with some of the modelling. IP assisted with  
279 site sampling and characterization, provided knowledge of the local geology, and  
280 helped develop our comments on seismic hazard. AM assisted with site sampling  
281 and characterization and contributed knowledge on the local geology, seismicity and  
282 geodesy, and advised on seismic hazard. ST helped to determine how to calculate  
283 differential stress from Coulomb stress. FI helped with discussions on interaction,  
284 seismic hazard and local geology, seismicity and geodesy. LC contributed to  
285 understanding of shear zone deformation, quartz flow laws and differential stress.  
286 KM helped with site characterisation and tectonic interpretations. RS ran the AMS for  
287 the  $^{36}\text{Cl}$  samples and helped with some field sampling. EV advised on local geology,  
288 seismicity, geodesy, and seismic hazard. All authors contributed to editing the  
289 manuscript.

290

## 291 **Methods**

292 *Inversion of slip histories from  $^{36}\text{Cl}$  cosmogenic dating:* Sites for cosmogenic  
293 sampling from limestone bedrock faults planes are carefully selected to ensure that



294 the scarps are formed solely by tectonic exhumation (see Supplementary Material 1  
295 which describes the characteristics of each sample site). A good site will have  
296 parallel hanging wall/footwall intersections with the fault plane, a smooth lower slope  
297 on the hanging wall devoid of erosional or depositional features, and will avoid active  
298 gullies or other erosional features present on the footwall or fault plane. 15 x 5 x 2.5  
299 cm sized samples of fault plane were taken parallel to the slip vector measured from  
300 frictional wear striations. These samples were prepared following the approach of  
301 refs.<sup>22,43</sup> and were analysed with AMS to determine the concentrations of <sup>36</sup>Cl in each  
302 sample. The concentration of <sup>36</sup>Cl increases up the fault plane as the length of time  
303 of exposure increases. We used the Bayesian MCMC code of ref.<sup>23</sup> to inverse model  
304 the slip history from measured concentrations of <sup>36</sup>Cl (results of the modelling are  
305 shown in Supplementary Material 2). This code searches for the probability  
306 distribution of the slip history conditioned on the measured data, and as an outcome  
307 identifies a slip history of best least-squares fit, while allowing a high flexibility of the  
308 magnitude and timings of slip events, uncertainties in the density of the colluvium  
309 and <sup>36</sup>Cl production factors, and timing of <sup>36</sup>Cl initial production. We have also  
310 iterated inputs, such as the total slip across the scarps (Supplementary Material 3),  
311 and find that the strain-rate and SRE results are relatively insensitive to uncertainty in  
312 these values. We also show that sample spacings on the fault planes we achieved  
313 are adequate to resolve the slip-rate changes we claim. We do this by progressively  
314 degrading the dense sampling for the Fiamignano fault to a point where two well-  
315 constrained historical earthquake sequences resolvable with the full data disappear  
316 (Supplementary Material 4). The full approach to the statistical modelling of slip  
317 histories using the <sup>36</sup>Cl data is described in <sup>23</sup>.

318

319 *Modelling Coulomb stress changes:* Non-planar strike-variable fault geometries are  
320 built as a series of rectangular elements<sup>44</sup> that are ~1km<sup>2</sup>. The geometry of the faults  
321 is based on extensive field data collected from limestone bedrock fault scarps in the  
322 central Apennines<sup>45-51</sup>. These strike-variable fault geometries are utilized in Coulomb  
323 3.4<sup>36</sup> to model Coulomb stress changes associated with earthquakes and slip on  
324 underlying shear zones. The brittle ductile transition is assumed to be at 15 km depth  
325 and shear zones are assumed to extend from 15 – 24 km depth<sup>3</sup>. For each fault, a  
326 characteristic earthquake magnitude is calculated using the relationship between  
327 fault area and magnitude<sup>52</sup>. A simple concentric slip distribution is calculated,  
328 assuming 40% of the maximum slip at depth reaches the surface, and the maximum  
329 slip is iterated to match the earthquake magnitude. The 40% assumption is based on  
330 iterating this value to closely match the ratios between (1) average subsurface

331 displacement and maximum surface displacement and (2) average subsurface  
 332 displacement and average surface displacement<sup>52</sup> (0.76 and 1.32 modal values  
 333 respectively). It is not possible to exactly match the modal values, the values  
 334 reported herein are within the variability reported<sup>52</sup>. The values used to calculate the  
 335 characteristic magnitude are given in Table 1.  
 336

Fault name	Fault length (km)	Fault dip (°)	Downdip length (km)	Fault area (km <sup>2</sup> )	M <sub>max</sub>	ASS/MS	ASS/AS	Max. slip (m)	Slip @ cosmo site (m)
Barete	19.7	42	22.4	441.6	6.66	0.71	1.41	2.40	0.64
Fiamignano	30.7	53	18.8	576.6	6.78	0.70	1.39	3.10	1.22
Laga	30.2	53	18.8	567.2	6.77	0.72	1.39	3.00	1.16
Leonessa	14.3	62	17.0	242.9	6.41	0.69	1.38	2.00	0.43
Mt Le Scalette	18.0	62	17.0	305.8	6.51	0.68	1.40	2.40	0.83
Vettore	32.9	63	17.0	558.9	6.76	0.69	1.32	3.20	1.13

337 Table 1 – Parameters used to calculate the characteristic earthquake magnitude  
 338 modelled on the faults discussed and to constrain the proportion of slip that occurs at  
 339 the surface compared to depth. The concentric slip distribution assumes a  
 340 symmetrical triangular surface slip distribution. ASS/MS = Average SubSurface  
 341 displacement/Mean Surface displacement. AS/MS = Average subsurface  
 342 displacement/Average Surface displacement

343  
 344 The contribution of each structure to the CST on the brittle faults is shown in  
 345 Supplementary Material 5. The annual magnitude of slip on underlying shear zones  
 346 is calculated from the Holocene throw profiles measured through fieldwork, as these  
 347 are suggested to be equivalent<sup>21</sup>.

348  
 349 *Calculating differential stress changes:* Coulomb stress changes are defined as  
 350  $\Delta\sigma_{CST} = \Delta\tau + \mu\Delta\sigma_n$ <sup>53</sup>, where  $\Delta\tau$  is the change in shear stress,  $\mu$  is the coefficient of  
 351 friction (herein 0.4 is used<sup>44</sup>) and  $\Delta\sigma_n$  is the change in normal stress. The shear  
 352 stress can be defined as  $\tau = \frac{1}{2}(\sigma_1 - \sigma_3)\sin 2\beta$ <sup>8</sup> where  $(\sigma_1 - \sigma_3)$  is the differential  
 353 stress and  $\beta$  is the angle between  $\sigma_1$  and the fault plane. In the central Apennines,

354 normal faulting is dominant and therefore we assume  $\sigma_1$  is vertical. Therefore  $\beta =$   
355  $90 - \theta$  where  $\theta$  is the dip of the fault. We have calculated the differential stress using  
356 the equations above and the shear stress calculated from Coulomb 3.4. The  
357 differential stress is calculated for each 1 x 1km rectangular fault patch for the brittle  
358 and ductile portions of the faults. The conversion between sig\_reverse (direct output  
359 from Coulomb 3.4) and differential stress is given in Supplementary Material 5.

360

361 *Calculating change in strain-rates:* Viscous deformation via dislocation creep, derived  
362 from laboratory experiments, is given by the following equation<sup>7</sup>:  $\dot{\epsilon} = Af_{H_2O}^m \sigma^n e^{-\frac{Q}{RT}}$ ,  
363 where  $\dot{\epsilon}$  is the strain rate,  $A$  is a material parameter,  $f_{H_2O}^m$  is the water fugacity,  $\sigma$  is  
364 the differential stress,  $n$  is the stress exponent,  $Q$  is the activation energy,  $R$  is the  
365 ideal gas constant and  $T$  is the temperature. For the dislocation creep of wet quartz<sup>7</sup>,  
366 the following constant values are used:  $A = 6.31e-12$  MPa/s,  $Q = 35$ kJ/mol<sup>7</sup>,  $R = 8.31$   
367  $m^2 \text{ kgs}^{-2}\text{K}^{-1}\text{mol}^{-1}$ ,  $n=3.26^3$ ,  $T = 710\text{K} / 440 \text{ }^\circ\text{C}^3$ ,  $f_{H_2O}^m = 110$  MPa (calculated given  $T =$   
368  $440 \text{ }^\circ\text{C}^3$  and pressure = 0.4GPa @15 km depth using the online fugacity  
369 calculator<sup>54,55</sup>). We choose this flow law for the following reasons: (a) dislocation  
370 creep mechanisms are common in natural quartz-bearing shear zones that dominate  
371 lower continental crust at the temperature and pressure range ascribed here<sup>37</sup>; (b)  
372 the chosen flow law<sup>7</sup> considers the effect of water fugacity and is relatively well-  
373 constrained via comparison to naturally deformed rocks; (c) the use of this flow law  
374 allows consistency with previous studies in this region from which we take the stress  
375 exponent<sup>3</sup>. We implement the calculations using Supplementary Material 6. Although  
376 the published flow law<sup>7</sup> uses  $n = 4$ , we substitute  $n = 3.26$  as derived for the  
377 Apennines region<sup>3</sup>. This has little effect on the resulting strain rate, which is the same  
378 order of magnitude at 10 MPa differential stress. The absolute value of differential  
379 stress is taken to be 10 MPa as values across this depth range are thought to be  
380 relatively uniform<sup>37</sup>. The change in differential stress is calculated from the Coulomb  
381 stress modelling. Sensitivity to the chosen values for differential stress and stress  
382 exponent are shown in Supplementary Material 7. Sensitivity to overestimating or  
383 underestimating the amount of slip across the scarps for strain-rates is shown in  
384 Supplementary Material 8. We converted the implied strain-rates for the shear zones  
385 into implied slip-rates and slip-rate changes for the overlying brittle faults by using (1)  
386 the ratio of strain-rates before and after the rate changes, and (2) the slip-rates over  
387 the entire observation period constrained in terms of timing from <sup>36</sup>Cl, and offset  
388 using scarp profiles at the surface (Supplementary Material 6). These long-term slip-  
389 rates were multiplied by the ratio of strain-rates before and after the rate changes,

390 and amounts of slip were recovered before and after slip-rate changes, by multiplying  
391 the ratio-modified slip-rates by the time periods in question. We used these values to  
392 compare measured and implied SRE values. We also show that implied earthquake  
393 recurrence intervals for 1 m slip events (typical of the region) are of reasonable  
394 duration (a few millennia from paleoseismology<sup>28,29,33</sup>), given the values we input into  
395 the quartz flow law, by calculating the recurrence intervals for 1m heave events,  
396 given that we can measure the across strike distance for the region, and can  
397 calculate heave rates before and after strain-rate changes assuming faults and shear  
398 zones dip at 45°. Supplementary Material 6 shows that recurrence intervals for 1 m  
399 heave events change from ~3.6 kyrs to ~10-19 kyrs during anticlusters, comparable  
400 in terms of order of magnitude to values from paleoseismology.

401

## 402 **References**

403

- 404 1. Sieh, K. *et al.* A more precise chronology of earthquakes produced by the San  
405 Andreas Fault in southern California. *J. Geophys. Res. Solid Earth* **94**, 603–  
406 623 (1989).
- 407 2. Pace, B. *et al.* Layered seismogenic source model and probabilistic seismic-  
408 hazard analyses in central Italy. *Bull. Seismol. Soc. Am.* **96**, 107–132 (2006).
- 409 3. Cowie, P. A. *et al.* Viscous roots of active seismogenic faults revealed by  
410 geologic slip rate variations. *Nat. Geosci.* **6**, 1036–1040 (2013).
- 411 4. Copley, A. *et al.* Unexpected earthquake hazard revealed by Holocene rupture  
412 on the Kenchreai Fault (central Greece): Implications for weak sub-fault shear  
413 zones. *Earth Planet. Sci. Lett.* **486**, 141–154 (2018).
- 414 5. Sibson, R. H. Fault rocks and fault mechanisms. *J. Geol. Soc. London.* **133**,  
415 191–213 (1977).
- 416 6. Roberts, G. P. & Michetti, A. M. Spatial and temporal variations in growth rates  
417 along active normal fault systems: An example from The Lazio-Abruzzo  
418 Apennines, central Italy. *J. Struct. Geol.* **26**, 339–376 (2004).
- 419 7. Hirth, G. *et al.* An evaluation of quartzite flow laws based on comparisons  
420 between experimentally and naturally deformed rocks. *Int. J. Earth Sci.* 77–87  
421 (2001). doi:10.1007/s005310000152
- 422 8. King, G. C. P. *et al.* Static stress changes and the triggering of earthquakes.  
423 *Bull. Seismol. Soc. Am.* **84**, 935–953 (1994).
- 424 9. Mildon, Z. K. *et al.* Coulomb pre-stress and fault bends are ignored yet vital  
425 factors for earthquake triggering. *Nat. Commun.* 1–9 (2019).  
426 doi:10.31223/osf.io/pt829

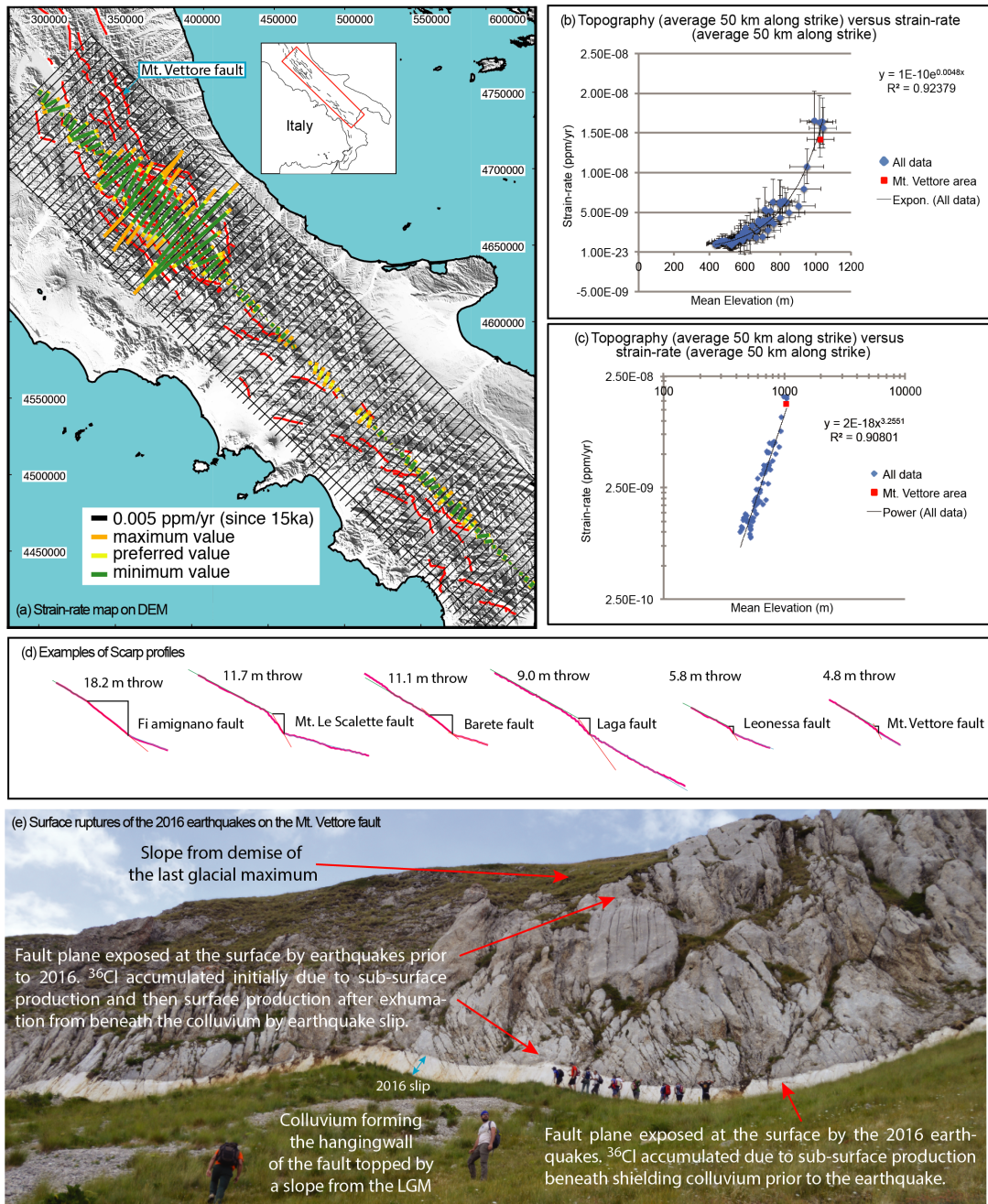
- 427 10. Cavinato, G. P. & De Celles, P. G. Extensional basins in the tectonically  
428 bimodal central Apennines fold-thrust belt, Italy: Response to corner flow  
429 above a subducting slab in retrograde motion. *Geology* **27**, 955–958 (1999).
- 430 11. Nijman, W. Tectonics of the Velino-Sirente area, Abruzzi, Central Italy, K.  
431 *Koninkl. Nederl. Akad. van Wet.* 156–184 (1971).
- 432 12. Doglioni, C. Some remarks on the origin of foredeeps. *Tectonophysics* **228**, 1–  
433 20 (1993).
- 434 13. D’Agostino, N. *et al.* Contemporary crustal extension in the Umbria-Marche  
435 Apennines from regional CGPS networks and comparison between geodetic  
436 and seismic deformation. *Tectonophysics* **476**, 3–12 (2009).
- 437 14. Selvaggi, G. Spatial distribution of horizontal seismic strain in the Apennines  
438 from historical earthquakes. *Ann. di Geofis.* **41**, (1998).
- 439 15. Anderson, H. & Jackson, J. Active tectonics of the Adriatic region. *Geophys. J.*  
440 *R. Astron. Soc.* **91**, (1987).
- 441 16. Chiaraluce, L. *et al.* The 2016 Central Italy Seismic Sequence: A First Look at  
442 the Mainshocks, Aftershocks, and Source Models. *Seismol. Res. Lett.* **88**,  
443 757–771 (2017).
- 444 17. Galli, P. *et al.* Twenty years of paleoseismology in Italy. *Earth-Science Rev.*  
445 **88**, 89–117 (2008).
- 446 18. Civico, R. *et al.* Surface ruptures following the 30 October 2016 Mw 6.5 Norcia  
447 earthquake, central Italy. *J. Maps* **14**, (2018).
- 448 19. Alessio, G. *et al.* Evidence for Surface rupture associated with the Mw 6.3  
449 L’Aquila earthquake sequence of April 2009 (central Italy). *Terra Nov.* **22**, 43–  
450 51 (2010).
- 451 20. Tucker, G. E. *et al.* Geomorphic significance of postglacial bedrock scarps on  
452 normal-fault footwalls. *J. Geophys. Res. Earth Surf.* **116**, 1–14 (2011).
- 453 21. Palumbo, L. *et al.* Slip history of the Magnola fault (Apennines, Central Italy)  
454 from <sup>36</sup>Cl surface exposure dating: Evidence for strong earthquakes over the  
455 Holocene. *Earth Planet. Sci. Lett.* **225**, 163–176 (2004).
- 456 22. Cowie, P. A. *et al.* Orogen-scale uplift in the central Italian Apennines drives  
457 episodic behaviour of earthquake faults. *Sci. Rep.* **7**, 1–10 (2017).
- 458 23. Beck, J. *et al.* Bayesian earthquake dating and seismic hazard assessment  
459 using chlorine-36 measurements (BED v1). *Geosci. Model Dev. Discuss.*  
460 **2018**, 1–24 (2018).
- 461 24. Galadini, F. & Galli, P. Paleoseismology of silent faults in the Central  
462 Apennines (Italy): The Mt. Vettore and Laga Mts. faults. *Ann. Geophys.* **46**,  
463 815–836 (2003).

- 464 25. Cinti, F. R. *et al.* 22-kyr-Long Record of Surface Faulting Along the Source of  
465 the 30 October 2016 Earthquake (Central Apennines, Italy), From Integrated  
466 Paleoseismic Data Sets. *J. Geophys. Res. Solid Earth* 1–28 (2019).  
467 doi:10.1029/2019jb017757
- 468 26. Guerrieri, L. *et al.* Evoluzione recente dea paesaggio e dissesto geologico-  
469 idraulico: primo risultati in un'area campione dell'Appennino Centrale (valle del  
470 Salto–Rieti). *Boll. della Soc. Geol. Ital.* **57**, 453–461 (2002).
- 471 27. Boncio, P. *et al.* Defining a model of 3D seismogenic sources for Seismic  
472 Hazard Assessment applications: The case of central Apennines (Italy). *J.*  
473 *Seism.* **8**, 407–425 (2004).
- 474 28. Galli, P. *et al.* Holocene paleoseismology of the Norcia fault system (Central  
475 Italy). *Tectonophysics* **745**, 154–169 (2018).
- 476 29. Galli, P. A. C. *et al.* Palaeoseismology of the L'Aquila faults (central Italy,  
477 2009, Mw6.3 earthquake): Implications for active fault linkage. *Geophys. J. Int.*  
478 **187**, 1119–1134 (2011).
- 479 30. Vittori, E. *et al.* Ground effects and surface faulting in the September-October  
480 1997 Umbria-Marche (Central Italy) seismic sequence. *J. Geodyn.* **29**, 535–  
481 564 (2000).
- 482 31. Michetti, A. M. & Serva, L. New data on the seismotectonic potential of the  
483 Leonessa Fault area (Rieti, central Italy). *Rend. della Soc. Geol. Ital.* **13**, 37–  
484 46 (1990).
- 485 32. Blumetti, A. M. Neotectonic investigation of evidence of paleoseismicity in the  
486 epicentral area of the January-February 1703, central Italy, earthquakes.  
487 *Perspect. Paleoseismology* **6**, 83–100 (1995).
- 488 33. Cinti, F. R. *et al.* Evidence for Surface Faulting Earthquakes on the Montereale  
489 Fault System (Abruzzi Apennines, Central Italy). *Tectonics* (2018).  
490 doi:10.1029/2017TC004780
- 491 34. Mildon, Z. K. *et al.* Coulomb stress transfer and fault interaction over millennia  
492 on non-planar active normal faults: the Mw 6.5-5.0 seismic sequence of 2016-  
493 2017, central Italy. *Geophys. J. Int.* **210**, (2017).
- 494 35. Reid, H. F. The mechanics of the earthquake. *Calif. Earthq. April 1906* **18**, 192  
495 (1910).
- 496 36. Toda, S. *et al.* Forecasting the evolution of seismicity in southern California:  
497 Animations built on earthquake stress transfer. *J. Geophys. Res. Solid Earth*  
498 **110**, 1–17 (2005).
- 499 37. Behr, W. M. & Platt, J. P. A naturally constrained stress profile through the  
500 middle crust in an extensional terrane. *Earth Planet. Sci. Lett.* **303**, 181–192

- 501 (2011).
- 502 38. Main, I. G. Earthquakes as Critical Phenomena: Implications for Probabilistic  
503 Seismic Hazard Analysis. *Bull. Seismol. Soc. Am.* **85**, 1299–1308 (1995).
- 504 39. Pace, B. *et al.* Do static stress changes of a moderate-magnitude earthquake  
505 significantly modify the regional seismic hazard? Hints from the L'Aquila 2009  
506 normal-faulting earthquake (Mw 6.3, central Italy). *Terra Nov.* **26**, 430–439  
507 (2014).
- 508 40. Dolan, J. F. *et al.* Extreme multi-millennial slip rate variations on the Garlock  
509 fault, California: Strain super-cycles, potentially time-variable fault strength,  
510 and implications for system-level earthquake occurrence. *Earth Planet. Sci.*  
511 *Lett.* **446**, 123–136 (2016).
- 512 41. Fay, N. & Humphreys, E. Dynamics of the Salton block: Absolute fault strength  
513 and crust-mantle coupling in Southern California. *Geology* **34**, 261–264  
514 (2006).
- 515 42. Dolan, J. F. *et al.* Long-range and long-term fault interactions in Southern  
516 California. *Geology* **35**, 855–858 (2007).
- 517 43. Stone, J. O. *et al.* Cosmogenic chlorine-36 from calcium spallation. *Geochim.*  
518 *Cosmochim. Acta* **60**, 679–692 (1996).
- 519 44. Mildon, Z. K. *et al.* Evaluating models of Coulomb stress transfer: Is variable  
520 fault geometry important? *Geophys. Res. Lett.* **43**, (2016).
- 521 45. Roberts, G. P. Visualisation of active normal fault scarps in the Apennines,  
522 Italy: a key to assessment of tectonic strain release and earthquake rupture. *J.*  
523 *Virtual Explor.* **29**, (2008).
- 524 46. Faure Walker, J. P. *et al.* Comparison of earthquake strains over  $10^2$  and  
525  $10^4$  year timescales: Insights into variability in the seismic cycle in the  
526 central Apennines, Italy. *J. Geophys. Res.* **115**, B10418 (2010).
- 527 47. Morewood, N. C. & Roberts, G. P. The geometry, kinematics and rates of  
528 deformation within an en echelon normal fault segment boundary, central Italy.  
529 *J. Struct. Geol.* **22**, 1027–1047 (2000).
- 530 48. Roberts, G. P. & Michetti, A. M. Spatial and temporal variations in growth rates  
531 along active normal fault systems: an example from The Lazio–Abruzzo  
532 Apennines, central Italy. *J. Struct. Geol.* **26**, 339–376 (2004).
- 533 49. Wilkinson, M. *et al.* Slip distributions on active normal faults measured from  
534 LiDAR and field mapping of geomorphic offsets: An example from L'Aquila,  
535 Italy, and implications for modelling seismic moment release. *Geomorphology*  
536 **237**, (2015).
- 537 50. Mildon, Z. K. *et al.* Active normal faulting during the 1997 seismic sequence in

- 538 Colfiorito, Umbria: Did slip propagate to the surface? *J. Struct. Geol.* **91**, 102–  
539 113 (2016).
- 540 51. Papanikolaou, I. D. *et al.* Fault scarps and deformation rates in Lazio–  
541 Abruzzo, Central Italy: Comparison between geological fault slip-rate and GPS  
542 data. *Tectonophysics* **408**, 147–176 (2005).
- 543 52. Wells, D. L. & Coppersmith, K. J. New empirical relationships among  
544 magnitude, rupture length, rupture width, rupture area, and surface  
545 displacement. *Bull. Seismol. Soc. Am.* **84**, 974–1002 (1994).
- 546 53. Harris, R. A. & Simpson, R. W. Changes in static stress on southern California  
547 faults after the 1992 Landers earthquake. *Nature* **360**, 251–254 (1992).
- 548 54. Withers, T. Fugacity calculator. (2019). Available at:  
549 <https://www.esci.umn.edu/people/researchers/withe012/fugacity.htm>.  
550 (Accessed: 11th March 2019)
- 551 55. Pitzer, K. S. & Sterner, S. M. Equations of state valid continuously from zero to  
552 extreme pressures for H<sub>2</sub>O and CO<sub>2</sub>. *J. Chem. Phys.* **101**, 3111–3116 (1994).
- 553 56. Faure Walker, J. P. *et al.* Relationship between topography, rates of extension  
554 and mantle dynamics in the actively-extending Italian Apennines. *Earth Planet.*  
555 *Sci. Lett.* **325–326**, 76–84 (2012).
- 556
- 557

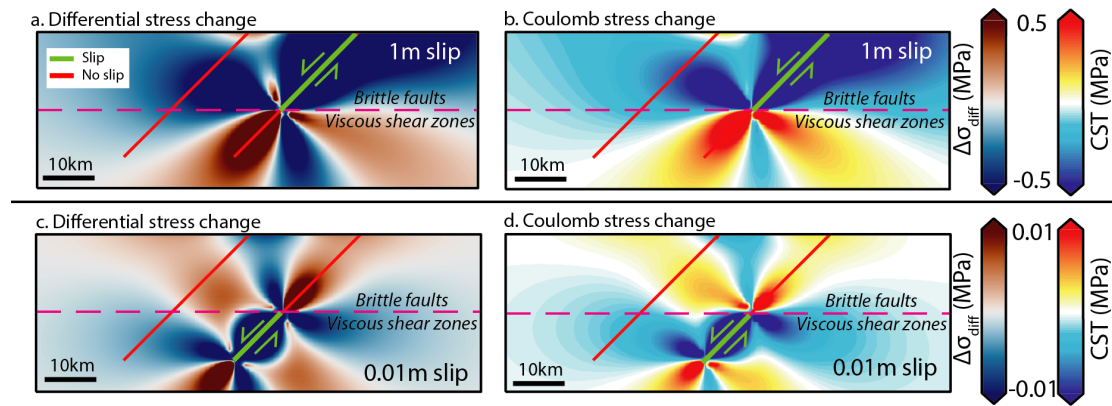




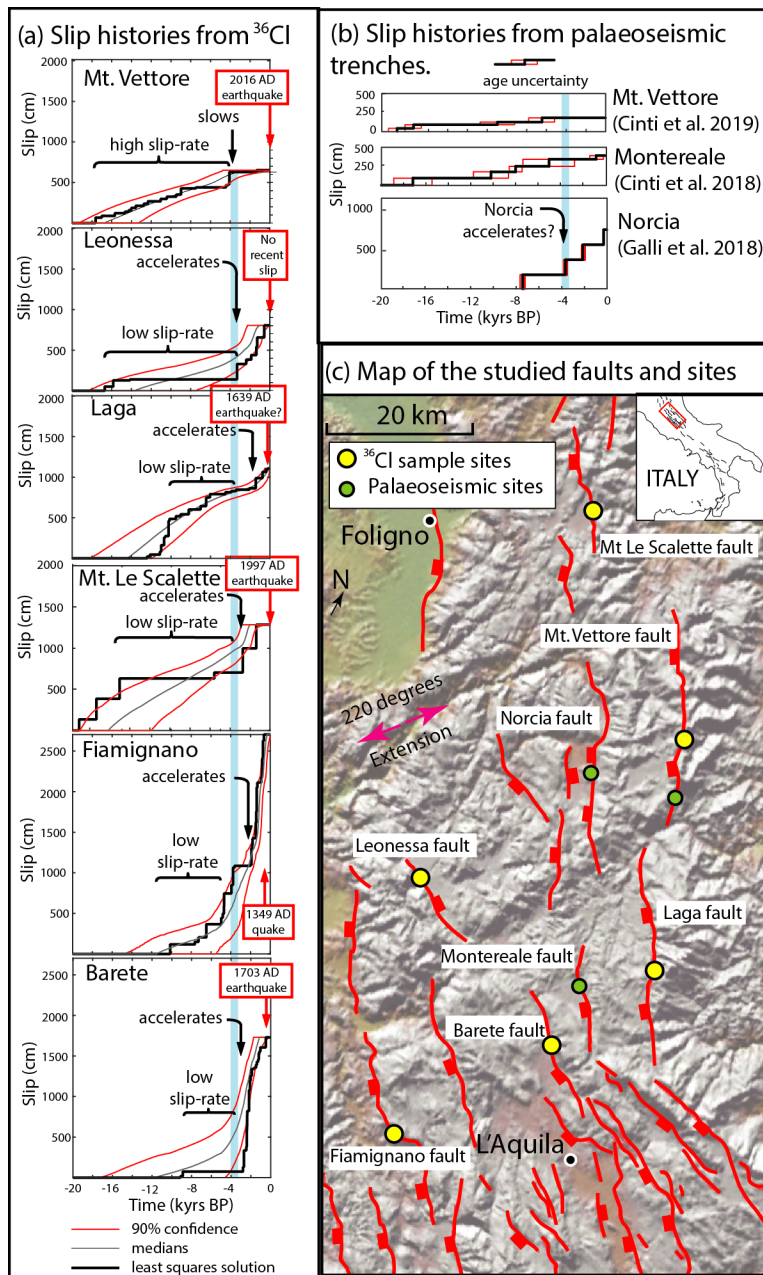
559

560 Fig. 1 – Current knowledge of fault and shear zone interaction in the central  
 561 Apennines. (a) Map showing the spatial variation in principal horizontal strain  
 562 calculated in 5×90 km boxes (black lines) traversing the Italian Apennines,  
 563 derived from the directions and magnitudes of faulted-offsets since 15 ±3 ka of  
 564 landforms dating from the demise of the Last Glacial Maximum, modified and  
 565 updated from ref.<sup>56</sup> (b) Mean elevation against strain rate from (a), showing a  
 566 power law correlation between datasets, updated from ref.<sup>3</sup>. (c) Log-log plot  
 567 of the data presented in (b), showing a power-law relationship with an  
 568 exponent of ~3.26; the value of this exponent implies that the brittle faults  
 are underlain and driven by viscous shear

569 zones. (d) Topographic profiles across active fault scarps used in this study. (e)  
 570 Surface ruptures of the 2016 earthquakes on the Mt. Vettore fault scarp showing how  
 571 slip on the brittle faults generates surface offsets and hence can be sampled for  $^{36}\text{Cl}$   
 572 analysis.  
 573



574  
 575 Fig. 2 – Cross-sections showing stress changes produced by slip in normal faulting  
 576 earthquakes and by slip on underlying shear zones. (a) and (b) show differential and  
 577 Coulomb stress resulting from a normal faulting earthquake; (c) and (d) show  
 578 differential and Coulomb stress resulting from slip in a viscous shear zone. Both  
 579 earthquakes and shear zone slip transfer negative differential stress (a reduction in  
 580 stress) onto the neighbouring shear zone, so a change in strain-rate on the receiver  
 581 shear zone is implied.  
 582

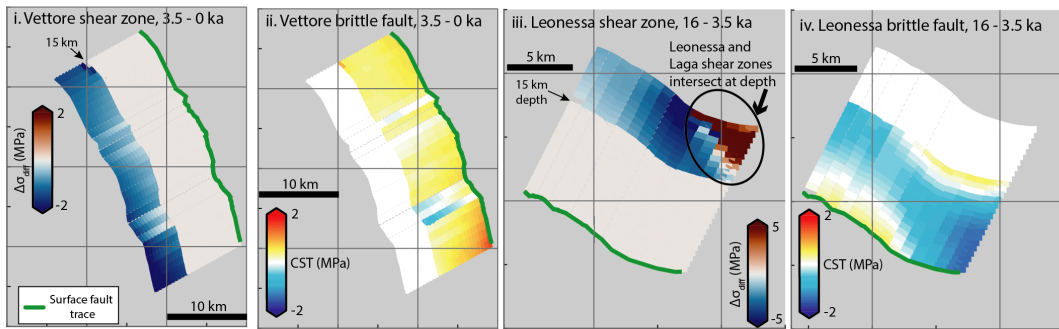


583

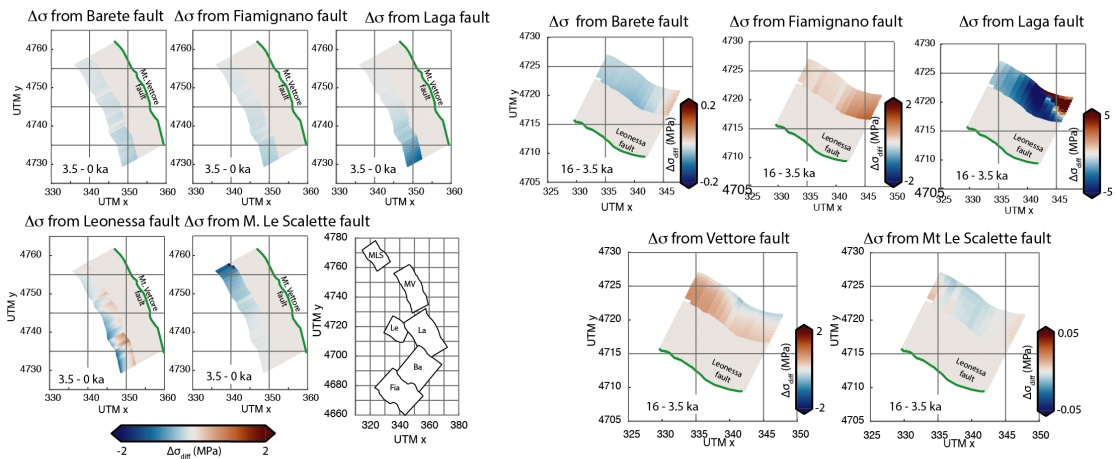
584 Fig. 3 – Slip histories for the studied active normal faults. (a) Slip histories derived  
 585 from *in situ*  $^{36}\text{Cl}$  cosmogenic exposure data for the six faults studied. At ~3.5 kyrs BP,  
 586 both the least squares slip histories and 90% confidence curves exhibit convex-  
 587 upward shapes for the Mt. Vettore fault and convex downward shapes for all the  
 588 other faults. Concavity indicates that slip-rates change for all the faults at ~3.5 kyrs  
 589 B.P.; the Mt. Vettore fault slows in activity and has a period of quiescence whilst all  
 590 the other faults accelerate. (b) Slip histories from other nearby faults from published  
 591 paleoseismic trenching that broadly agrees with our cosmogenic data. (c) Map  
 592 showing the locations of the faults studied,  $^{36}\text{Cl}$  sample sites and paleoseismic  
 593 trenches. The change in slip rate evidenced by the  $^{36}\text{Cl}$  slip histories is investigated

594 to determine whether it could be caused by changes in differential stress and hence  
 595 strain-rate in the underlying shear zones.  
 596

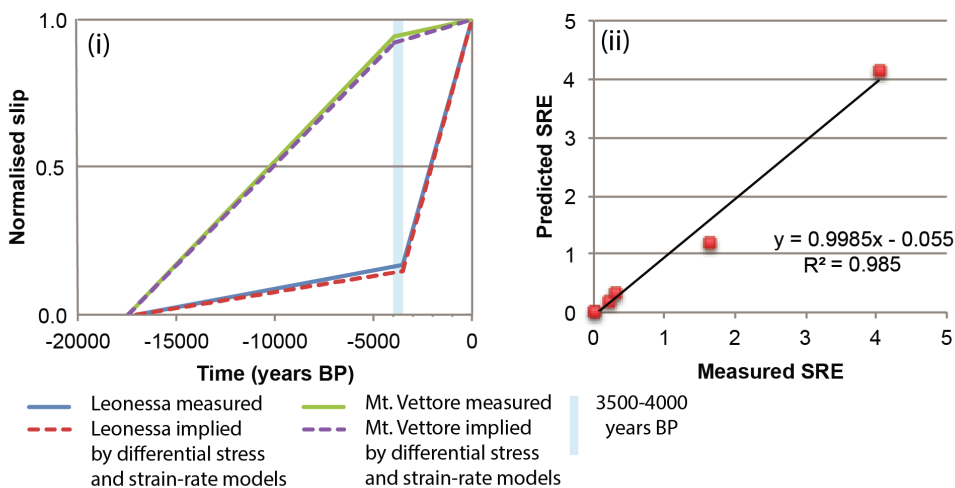
(a) Changes in differential stress on shear zones and CST on brittle faults from the combined action of all the other structures



(b) Contributions to changes in differential stress on shear zones from individual structures



(c) Comparison of measured slip histories and those implied by modelling



597

598 Fig. 4 – Stress changes and effects on slip rates during periods of quiescence for the  
 599 Mt. Vettore and Leonessa faults. (a) Cumulative changes in differential and Coulomb  
 600 stress on the Mt. Vettore and Leonessa faults. The periods of quiescence are shown  
 601 in the slip histories in Fig. 3. (b) Contributions to the cumulative differential stress

602 from individual neighbouring faults studied with  $^{36}\text{Cl}$  analysis, with (a) as the sum of  
603 all the values shown in this panel. (c) Comparison between measured slip histories  
604 from  $^{36}\text{Cl}$  and slip histories inferred from differential stress changes and the quartz  
605 flow law. Values are normalised to the total measured slip. Slip Rate Enhancement  
606 (SRE) values are calculated relative to the long-term ( $15 \pm 3\text{kyr}$  rate) slip rate, where  
607  $\text{SRE} < 1$  implies a slowing of slip and a reduction in activity. The similarity between  
608 measured and implied slip histories suggests the approach we use, combining stress  
609 changes with quartz flow laws, to generate the implied slip histories replicate the  
610 natural system.